JTTEE5 7:349-356

PEER REVIEWED

Fluid Dynamic Study of Direct Current Plasma Jets for Plasma Spraying Applications

M. Rahmane, G. Soucy, M.I. Boulos, and R. Henne

(Submitted 23 October 1997; in revised form 17 March 1998)

Recently, direct current (dc) plasma torches equipped with converging-diverging (Laval) nozzles, instead of standard cylindrical ones, have been shown to present several advantages for both vacuum and atmospheric plasma spraying, such as diminishing the gradients of temperature and velocity and reducing the turbulence intensity in the jet fringes. The present study was concerned with the diagnostics of the plasma jets produced by three nozzles of various contours: a standard cylindrical anode and a Mach 2.5 and Mach 3 Laval nozzle. Emission spectroscopy (absolute intensity) and enthalpy probe techniques were used to measure temperature and velocity fields. Special attention was given to the effects of spray chamber pressure on flow regime inside the nozzles and to the distribution of the temperature and velocity fields in the plasma jet. Results showed that under the chamber pressure conditions used (vacuum), for which Laval nozzles originally were designed, the generated plasma jets had greater centerline velocities and larger high temperature zones compared to standard cylindrical nozzles. The results showed significant improvement in the deposition efficiency by using nozzles with these computed contours.

Keywords compressible flows, diagnostics, laval nozzles, plasma spray, thermal plasmas

1. Introduction

With the aim of improving deposition efficiency and coating quality produced by direct current (dc) plasma spraying process, it was found that plasma jets with a relatively large hot core and flat temperature and velocity profiles were preferable to ensure uniform treatment of the powder. Moreover, the powder injection setup and conditions must be favorable for the entry of powder particles into the central region of the jet, which should take place as close as possible to the plasma generation source.

Conventional dc plasma torches equipped with standard nozzles of cylindrical shape do not provide the most favorable particle melting and acceleration conditions for injected powders. Plasma jets generated by such nozzles at atmospheric pressure are dominated by strong interactions with the surroundings. The relatively cool ambient gas entrained by the jet to its central core is responsible for the rapid cooling and deceleration of the plasma flow (Ref 1, 2). These aspects, combined with the typical jet properties of a narrow hot core and strong radial temperature gradients, render the process particularly sensitive to the powder injection conditions. Elaborate powder injectors, whether internal or external to the torch, and stringent requirements on particle size distribution of the powder often have been necessary to optimal control of the quality of deposits obtained.

The use of standard nozzles under vacuum conditions results in jet overexpansion and the formation of so-called Mach knots under supersonic flow conditions. The pressure oscillations and the extended surface of the jet, due to the presence of the knot, lead to stronger interaction with the surrounding gas and hence to relatively rapid decay in flow velocity and increased cooling of the plasma.

In several conventional dc plasma torch designs, a rotational motion is introduced in the gaseous envelope enclosing the plasma flow to increase the arc voltage and hence to increase plasma enthalpy. The plasma gas is swirled in these cases as it enters the discharge chamber by means of holes helically drilled into the plasma gas distribution ring placed around the cathode. This causes an intense cross-interactional cooling between the cold injected gas and the discharge, forcing the discharge to become narrower and screw-like in form (Ref 3). The anodic spot (arc root) of the discharge is thus forced to rotate, which prevents local overheating and destruction of the inner anode wall. However, plasma rotation within the torch also affects the free plasma jet emerging from the torch. The plasma jet (or at least its envelope) rotates so that the radially injected powder particles are diverted around the jet and thus prevented from entering the jet core (Ref 3).

With the above improvements to the spray process, the following benefits can be expected:

- Extension of the hot plasma core, combined with a simultaneous reduction of the axial peak plasma temperature
- Reduction of the plasma jet temperature and velocity gradients
- Reduction of the level of turbulence in the jet
- Prevention of shock waves
- Reduction or suppression of the swirling nature of the plasma jet envelope at the exit of the torch nozzle without compromising the internal rotation of the arc root in the anode region

In this article, special attention is given to the use of contoured, Laval-type nozzles as a means of controlling the characteristics of the plasma jet. Plasma temperatures and flow

M. Rahmane, G. Soucy, and **M.I. Boulos,** Plasma Technology Research Centre (CRTP), Department of Chemical Engineering, Université de Sherbrooke, Québec, J1K 2R1, Canada; and **R. Henne,** DLR Institute for Technical Thermodynamics, Stuttgart, Germany. Contact e-mail: boulos@plasma.gcm.usherb.ca.

velocities are measured for plasma jets generated by standard dc plasma torches equipped with nozzles of various contours, e.g., cylindrical and Laval profiles. The diagnostic techniques used include enthalpy temperature (up to 10,000 K) and velocity measurements, emission spectroscopy (absolute intensity) for temperatures above 9000 K, and mass spectrometry for plasma composition analyses. The effects of nozzle contours and spray chamber pressure on the plasma flow properties are examined.

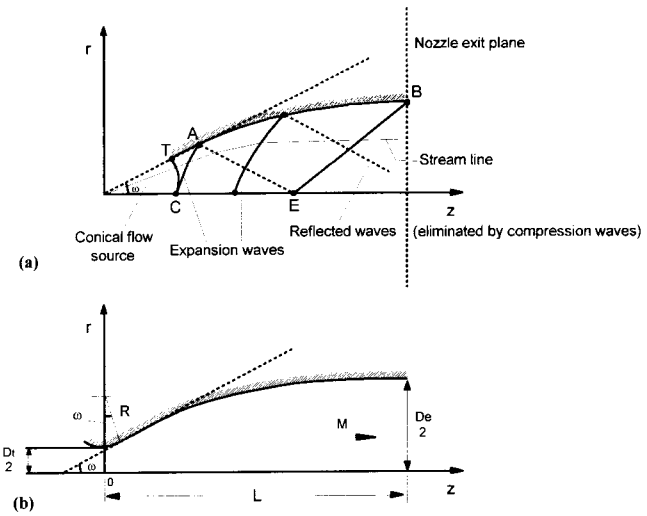

Fig. 1 (a) Conversion of radial flow into a parallel flow. (b) Axially symmetric Laval nozzle for a parallel and uniform flow (Ref 4)

2. Design of Laval Nozzle Contours

Converging-diverging nozzles have the potential to generate supersonic flows if the pressure ratio across the nozzle is higher than its critical value (upstream pressure (p_i)/ambient chamber pressure (p_a) $\cong 0.5$). To obtain a parallel flow or a jet free of compression and expansion waves (Mach knots) within the nozzle, the nozzle interior contour must possess a special design. Such nozzles, providing uniform and parallel flows, have long been required for wind tunnels and for jet propulsion. Seventy years ago, two-dimensional nozzles were designed by means of

Table 1 Typical data for Laval nozzle design (without boundary layer correction)

	Air, γ = 1.4				Argon, γ = 1.67			
M	1.5	2.0	2.5	3.0	1.5	2.0	2.5	3.0
ω (deg)	3.0	6.6	9.8	12.4	2.6	5.5	7.8	9.7
D_e/D_t	1.09	1.30	1.62	2.05	1.07	1.24	1.46	1.73
A_e/A_t	1.18	1.69	2.64	4.22	1.15	1.53	2.13	3.00
L/D_e	1.33	1.90	2.30	2.66	1.32	1.91	2.34	2.71

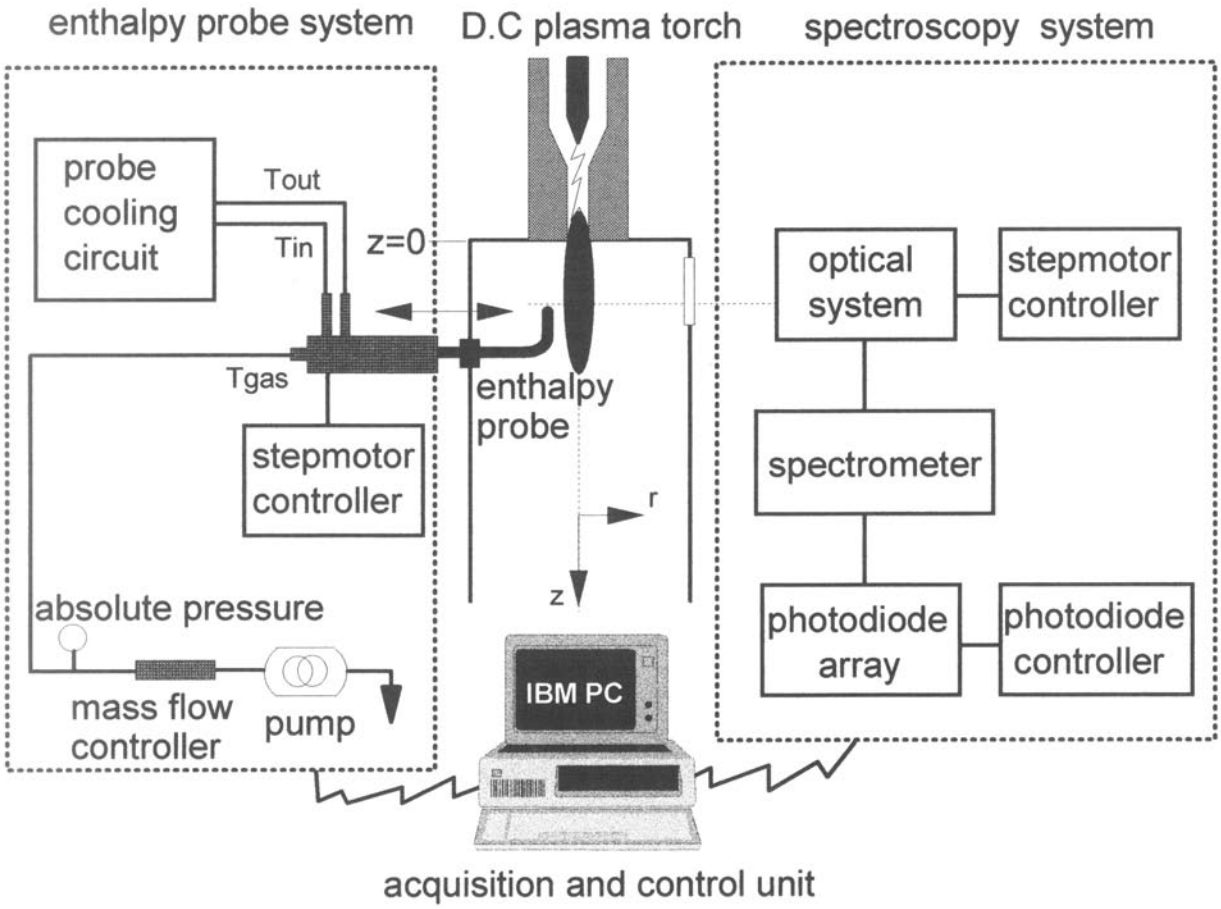

Fig. 2 Experimental setup

graphical methods. The graphical design of nozzles with axial symmetry represented an even more difficult and time-consuming problem. A simplified method using successive approximations was proposed by Foelsch (Ref 4). Equations for the contours of an axially symmetric Laval nozzle were derived by integration of the characteristic equations of the axially symmetric flow. Because these equations could not be integrated in a mathematically exact and closed form, it was necessary to find an approximation, which was achieved by matching the conditions of the flow at the end of the initial conical section with that at the beginning of the Laval profile combined with the linearization of the characteristic equations.

The primary function involves the derivation of the equation for the transition curve by which the conical source flow coming from the sonic section (see Fig. 1a) is converted to a parallel and uniform flow. The second step takes into consideration that the flow at the throat is usually plane and not spherically curved.

Typically, the compression and expansion waves originating from the wall and the source of the flow are studied. The flow streamlines are deflected at these waves depending on the character of the wave, i.e., at compression waves, deflection occurs toward the wave line, and at expansion waves, deflection away from the wave line. Expansion waves originate from wall segments with convex curvature, whereas compression waves can arise from the concave parts of the wall. Waves striking a wall are reflected in a manner corresponding to the reflection law. To obtain a parallel flow at the nozzle exit, the curvature of the wall along A to B (Fig. 1a) must be positioned so that the reflected waves of the incoming expansion waves are superimposed on and eliminated by the compression waves originating from this spot. Foelsch (Ref 4) analytically describes the flow field and transition curve interactions. He also provides the equations and data needed to calculate the coordinates of the nozzle wall to produce a flow parallel to the axis. Figure 1(b) schematically depicts the contour of such a nozzle.

Typical data for these nozzles (Fig. 1b) are given in Table 1 for several Mach numbers (M) and for two different values of γ (ratio of specific heats: $\gamma = C_p/C_v$).

3. Experimental Procedures

A schematic diagram of the experimental setup used in the present study is shown in Fig. 2. The setup consisted of a dc plasma torch system, an enthalpy probe system, and an emission spectroscopy apparatus. The dc plasma torch was constructed with a water-cooled copper anode and a thoriated tungsten cathode. The Laval nozzles, with Mach numbers of 2.5 and 3, were designed using standard methods which are based on several assumptions such as isentropic flow, thermodynamic equilibrium, and the absence of a boundary layer. Typical nozzle dimensions are shown in Fig. 3.

Because the three anodes tested have different lengths, a common reference point was assigned, so that the measured profiles of the plasma jet temperature and velocity of the three nozzles could be compared at a specified axial location. The axial zero ($z = 0$) level was set at the exit plane of the standard cylindrical anode (N1).

The plasma jet discharges into a water-cooled chamber equipped with quartz windows to observe the jet. A sealed scanning mechanism provides for radial movement of the probe. The axial location of the probe with respect to the plasma jet nozzle was adjusted by moving the torch vertically. The plasma torch was operated with an Ar/H_2 (1 vol% H_2) mixture as the plasma gas, at a total gas flow rate of 50 slpm. The arc current was 400 A and voltage was 40 V. The chamber pressure could be adjusted between 1 and 100 kPa.

The emission spectroscopy study was carried out by means of a 1-m Jobin-Yvon (Jobin-Yvon, Cedex, France) monochromator fitted with a grating with 1200 grooves/mm, thus providing a linear dispersion of 0.78 nm/mm. The output signal was received by a photodiode array in the monochromator output plane. In the vertical position, the photodiode array recorded the signal corresponding to the light emitted by the plasma jet in the lateral direction. The absolute intensity of the radiation was obtained by calibration against a standard tungsten filament lamp. The determination of local values of the emitted intensity was undertaken by means of the Abel inversion. Further details on the emission spectroscopy measurement technique are given in Ref 5.

The enthalpy probe system included a water-cooled stainless steel probe, a closed loop deionized cooling water circuit, a gas sampling line equipped with an appropriate mass flow controller, and a data acquisition and control unit, interfaced with LABVIEW (National Instruments, Austin, TX) software. A mass spectrometer was connected to the gas line to measure the gas concentration. The enthalpy probe had an outer diameter of 4.78 mm and an inner diameter of 1.27 mm. It was made from three concentric stainless steel tubes. The probe cooling system consisted of a variable-speed positive-displacement pump with

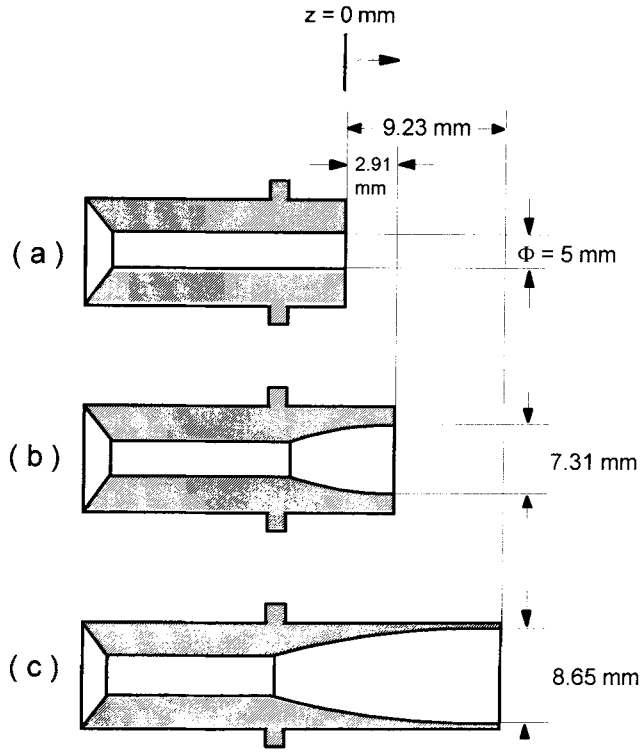

Fig. 3 Contours and dimensions of the cylindrical nozzle (N1), Laval Mach 2.5 nozzle (N2), and Laval Mach 3 nozzle (N3)

a maximum delivery rating of 0.8 L/min. To prevent boiling in the probe, the water cooling circuit was operated at a pressure of 6 MPa. On exiting the probe, the cooling water passes through a double tube heat exchanger, before going to the pressure intensifier, followed by the recirculation pump.

Calibration of the enthalpy probe system was described in a previous study (Ref 6). Errors associated with the measurements of plasma enthalpy and velocity by the probe were estimated to be ±7%. A detailed analysis of the uncertainty associated with such measurements is given in Ref 6-9; consequently, only the basic equations will be given here. The value of local specific enthalpy (h_i) of the plasma flow can be derived from an energy balance on the cooling water circuit as given by the equation:

$$h_i = h_e + \frac{\dot{m}_w}{\dot{m}_g} C_p (\Delta T_{\text{sampling}} - \Delta T_{\text{tare}}) \quad \text{(Eq 1)}$$

where h_e is the specific enthalpy of the sampled plasma gas at the probe exit; $\dot{m}_w$ and $\dot{m}_g$ are the mass flow rates of the cooling water and the sampled plasma gas, respectively; C_p is the specific heat of water, and ΔT is the increase in the cooling water temperature. The subscripts "tare" and "sampling" refer to the temperature measurements made during the tare measurement and under sampling conditions, respectively.

The probe also may be used as a water-cooled Pitot tube for stagnation pressure (p_o) measurement. At low Mach numbers (M < 0.3) the flow may be considered to be incompressible and the axial velocity (U) is deduced from the Bernoulli equation:

$$U = \sqrt{\frac{2(p_o - p_a)}{\rho(T)}} \quad \text{(Eq 2)}$$

where p_a is the ambient pressure in the chamber and $\rho(T)$ is the density of the plasma gas at its local sampling temperature.

If the Mach number is high (M > 0.3), the flow is considered compressible, and the kinetic energy of the plasma cannot be overlooked in comparison to its enthalpy. In this case, the free stream enthalpy (h), axial velocity (U), and Mach number (M) are determined through iterative solution of the following equations:

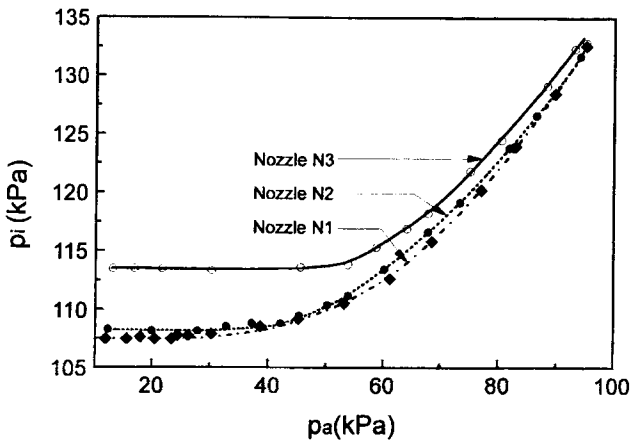

Fig. 4 Variation of upstream pressure (inside the nozzles) as a function of ambient chamber pressure. Plasma gas: Ar/H_2 (1 vol% H_2) at 45 slpm. Torch voltage and current: 35 V and 400 A

$$h = h_i - \frac{U^2}{2} \quad \text{(Eq 3)}$$

$$U = M\sqrt{\gamma RT} \quad \text{(Eq 4)}$$

$$\frac{p_o}{p_a} = \left(1 + \frac{\gamma - 1}{2} M^2\right)^{\gamma/(\gamma-1)} \quad \text{(Eq 5)}$$

where h_i is the stagnation enthalpy of the flow; γ is the specific heat ratio; and R is the composition-dependent gas constant.

4. Results and Discussion

4.1 Measurement of Critical Sonic Pressure Ratio

To identify the flow regime within the nozzles, the upstream pressure, p_i (inside the anode, close to the cathode tip), is measured as a function of the variation in chamber pressure, p_a. The results are shown in Fig. 4. For the three nozzles tested (N1, N2, and N3), the value of the critical sonic pressure ratio was found to be about 0.44, which is in good agreement with the theoretical value of 0.48, which was calculated using Eq 6 for isentropic flow conditions:

$$\left(\frac{p_i}{p_a}\right)^* = \left(\frac{\gamma + 1}{2}\right)^{\gamma/(\gamma-1)} \quad \text{(Eq 6)}$$

For the standard anode (N1), when the discharge pressure p_a is decreased below the critical value (45 kPa), the upstream pressure p_i remains constant, and visible shock waves are observed in the plasma jet beyond the nozzle exit plane. The shock waves are an indication of sonic flow inside the N1 nozzle. However, for the N2 and N3 nozzles (expanding nozzles), the shock waves were not visible even at chamber pressures below 45 kPa, despite the existence of supersonic flow conditions based on the critical pressure ratio criteria.

4.2 Temperature and Velocity Profiles

The radial profiles of temperature and velocity are measured at different axial locations using the nozzles N1, N2, and N3. For the operation of each nozzle, the chamber pressure was adjusted sequentially to the values 27, 53, and 78 kPa. A summary of the cases investigated is given in Table 2.

Comparison of Enthalpy Probe Results with Emission Spectroscopy Measurements. The radial temperature profiles obtained at a chamber pressure of 53 kPa are presented in Fig. 5 for the three test nozzles. Because of the high heat flux to which the probe was exposed in the high-temperature region, enthalpy probe measurements were limited to an axial location equal to or greater than 35 mm from the standard anode exit plane. Emission spectroscopic techniques, on the other hand, generally are not reliable at temperatures below 9000 K (Ref 10). Accordingly, the use of emission spectroscopy was limited to distances less than 45 mm from the exit plane of the plasma jet. Overlap between the two techniques was thus limited to two profiles. As

shown in Fig. 5, for nozzles N1 and N2, there is reasonable agreement between the results of the two techniques at axial positions of 35 and 45 mm, whereas for N3 agreement between the two measured temperature profiles was limited to the core zone of the plasma jet. A distinct discrepancy was observed between the results of the two methods in the vicinity of the fringes and downstream regions of the plasma jet. This finding was consistent with earlier data reported by Pfender and co-workers (Ref 1 and 11), who explained the phenomena by the fact that cool surrounding gases are entrained from the fringes and transported toward the jet centerline. Emission spectroscopy (absolute intensity) measurements make reference only to the hot plasma temperature, whereas enthalpy probes measure the average temperature of the hot plasma and the cool entrained gases.

Figure 6 illustrates the enthalpy probe measurements of radial profiles of the plasma velocity for the three nozzles at 53 kPa, at the same axial positions as above. Note that the central value of the plasma velocity decreases when the nozzle profile changes from the N1 contour to N3. On the other hand, the Mach values on the centerline (Table 2) indicate that, under the present operating conditions of the plasma torch (see Fig. 4), the flow resulting from the three nozzles were subsonic (in the investigated regions of the jet) when the chamber pressure was above 45 kPa. Because of the presence of these subsonic flow conditions and

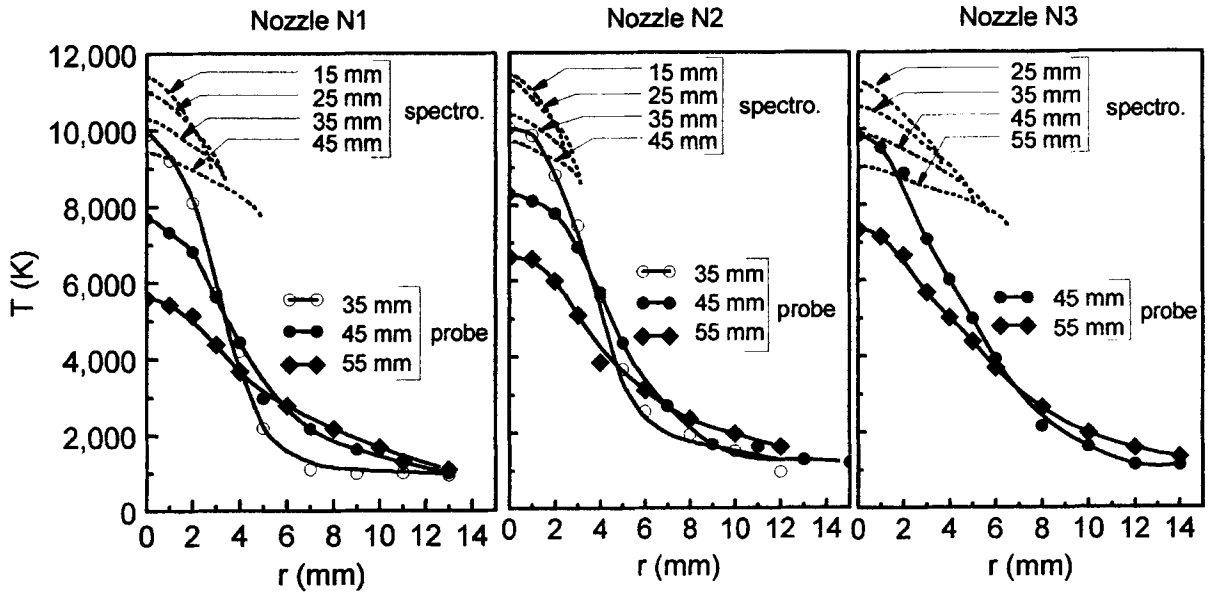

Fig. 5 Enthalpy probe and emission spectroscopy (absolute intensity) measurements of the radial temperature profiles at different axial locations for the N1, N2, and N3 nozzles (p_a = 53 kPa)

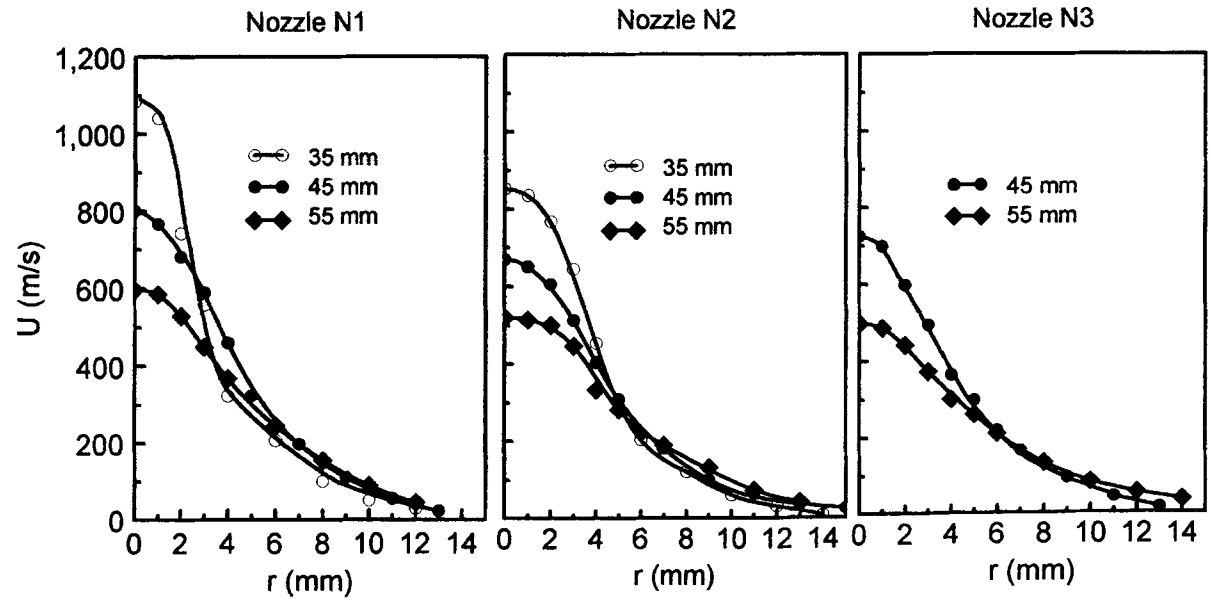

Fig. 6 Enthalpy probe measurements of radial profiles of the velocity at different axial locations for the N1, N2, and N3 nozzles (p_a = 53 kPa)

enlargements in the inner diameter of the nozzles (Fig. 3), the plasma velocity was necessarily reduced, in conformity with Bernoulli's law.

Influence of Nozzle Profile and Chamber Pressure. The enthalpy probe measurements of temperature and velocity profile (Fig. 7 and 8) indicate that at 27 kPa, where supersonic flow conditions exist, the N3 nozzle provided not only a larger plasma jet hot core, but also a higher centerline value for flow velocity, compared to the corresponding values for the N2 and N1 nozzles. Similar observations were found at 53 and 78 kPa for the temperature profiles (Fig. 7). At 78 kPa, however, the sequence of the N2 and N3 curves changed, and the centerline temperature for the N3 curve was lower. However, it can be expected that in the case where technical spray parameters are considered, e.g., where torch power is above 30 or 40 kW, an enlarged hot zone will exist even under atmospheric pressure conditions when using the N2 and N3 nozzles.

Figure 7 also indicates that, for the nozzles investigated, increases in the chamber pressure from 27 to 78 kPa resulted in lower centerline temperature values at the same axial location (55 mm). This is due to the fact that the plasma jet becomes shorter at higher pressures because of decreased flow velocities. The radial profiles of plasma velocity at 27 kPa are presented in Fig. 8. The central region values of flow velocity for the N2 and N3 nozzles are higher than those for the N1 nozzle. However, the opposite effect is observed at the 53 and 78 kPa conditions. This influence of pressure can be explained by the supersonic flow conditions that exist at 27 kPa within the Laval N2 and N3 nozzles and the subsonic flow conditions that prevail at higher pressure (53 and 78 kPa).

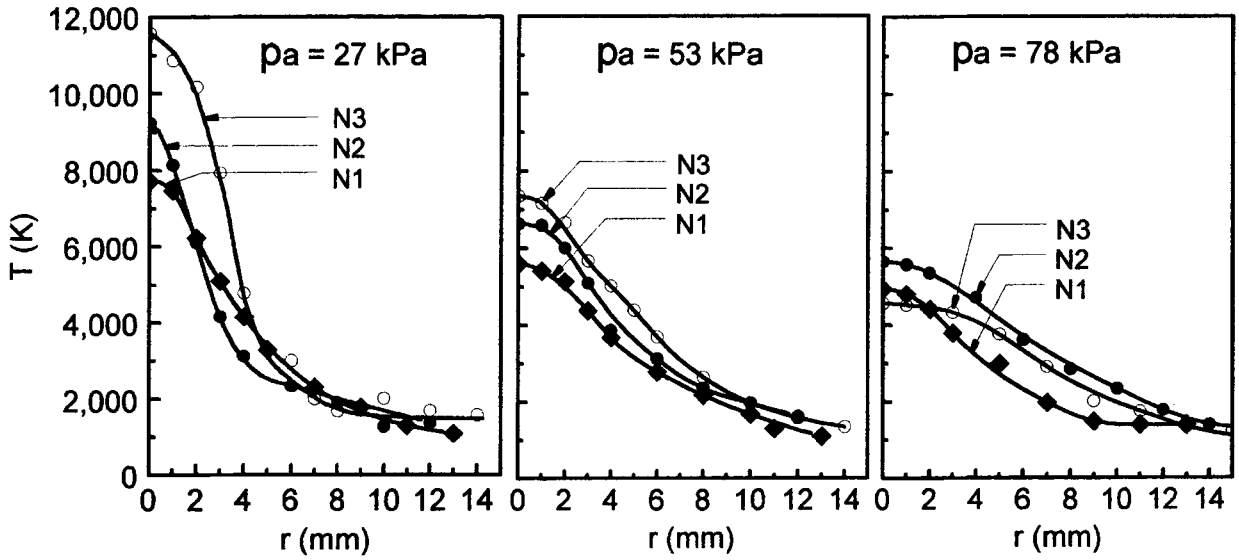

Fig. 7 Effect of nozzle profile on the temperature field at different chamber pressures (z = 55 mm)

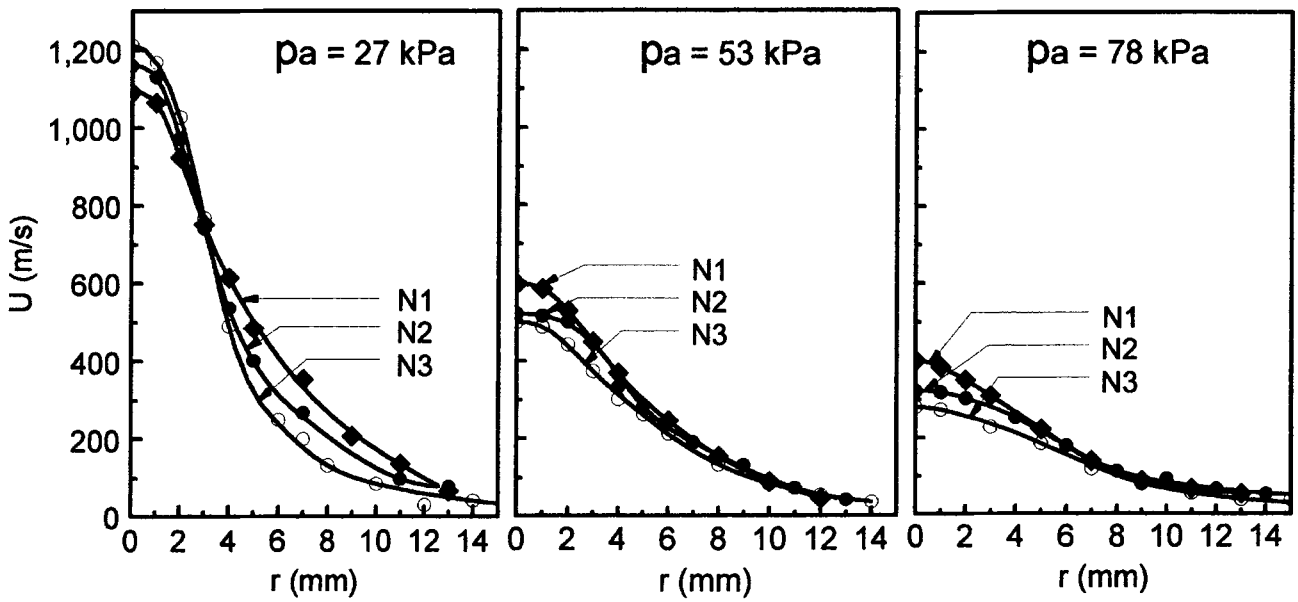

Fig. 8 Effect of nozzle profile on the velocity field at different chamber pressures (z = 55 mm)

As indicated in Table 2, Mach values at 27 kPa are still above 0.6 for the three nozzles, even at axial locations as far as 55 mm. These findings indicate the existence of a transonic region between $z = 0$ and $z = 55$ mm and confirm the presence of high temperature and velocity gradients in this case. Thus, the plasma jet passes rapidly from supersonic flow at the exit of the nozzle to a subsonic regime within a short distance. Nevertheless, with the Laval nozzle, the radial velocity and temperature profiles exhibit a larger uniform core compared to those produced by the standard nozzle.

4.3 *Influence of Nozzle Profile on Characteristics of Plasma Sprayed Coatings*

For various reasons, it is of interest to know whether nozzles designed primarily for supersonic flow conditions can also be operated satisfactorily at atmospheric pressure with subsonic flows and jet velocities, for example, to operate consecutively with the same nozzle at both low (vacuum) and high (atmospheric) pressures. One specific task in this regard concerns the spraying of thermal barrier coating systems, which consist of a bond coating (MCrAlY), preferably sprayed under vacuum plasma spraying (VPS) and high-velocity conditions for jets and particles, followed by the barrier coating (stabilized zirconia) sprayed at atmospheric pressure and under subsonic conditions. For this reason, various ceramic powders were sprayed with such nozzles at atmospheric pressure to gain knowledge of the resulting coating qualities and deposition efficiencies. Figures 9(a) and (b) illustrate the influence of nozzle geometry on the layer structure of an atmospheric plasma-sprayed $Al_2O_3 \cdot 3TiO_2$ (–45+5.6 μm) coating. Figure 9(a) is a micrograph of a deposited coating obtained with the cylindrical nozzle (N1), and Fig. 9(b) shows a micrograph of a deposited coating that resulted from the use of an expanded nozzle (N2). In both cases, the dc plasma torch was operated with Ar (35 slpm) + H_2 (10 slpm) as the plasma gases at an arc current of 600 A. For the N2 nozzle, the arc voltage was only 59 V compared to 66 V for the N1 nozzle when using the same gas and current parameters. Although the plasma power level was only 35.4 kW (N2 nozzle), and hence significantly lower in comparison with the 39.6-kW plasma power level for the N1 nozzle, the observed deposition efficiency was higher by about 10% when using the expanded nozzle. Furthermore, the coatings deposited with the expanded nozzle were of much greater density (Fig. 9a and b).

Table 2 Summary of experimental data

Nozzle No.	Test No.	Chamber pressure, kPa	Enthalpy probe axial location, mm	Mach number(a)
N1	1	27	55	0.68
	2	27	70	...
	3	53	35	0.58
	4	53	45	0.49
	5	53	55	0.42
	6	78	45	...
	7	78	55	0.30
N2	8	27	55	0.65
	9	27	70	...
	10	53	35	0.45
	11	53	45	0.39
	12	53	55	0.34
	13	78	55	0.23
N3	14	27	55	0.61
	15	27	70	...
	16	27	85	...
	17	53	45	0.39
	18	53	55	0.31
	19	78	45	...
	20	78	55	0.22

(a) Mach numbers are calculated for pure argon plasma at the local temperature, velocity, and composition at the measurement point.

Improvements to coating quality and deposition efficiency are clear indications of the more favorable conditions prevailing for plasma/powder particle interaction, in terms of both heat and momentum transfer. This has been achieved by the use of the computed Laval contour nozzles, thus resulting in extended cross sections of the hot jet core, moderated gradients, and reduced interaction of the jet with the cold gas surroundings.

5. Conclusions

Under the reported operating conditions of the plasma torch (plasma power and plasma gas flow rate), the plasma

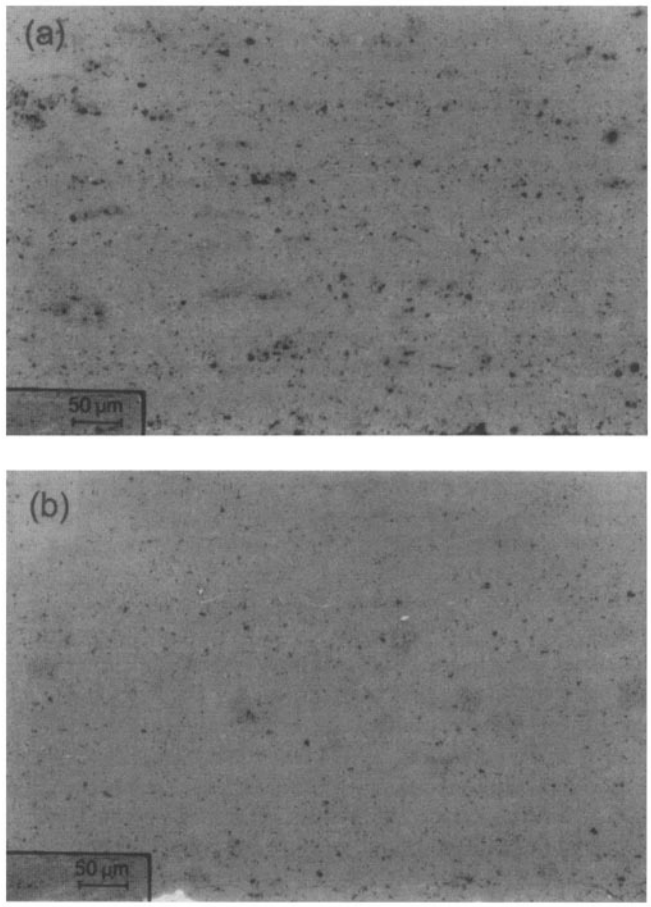

Fig. 9 $Al_2O_3 \cdot 3TiO_2$ layers produced by atmospheric plasma (Ar/H_2) spraying, using (a) standard nozzle, plasma gas, 35 slpm (Ar) + 10 slpm (H_2), 600 A, 66 V; and (b) Mach 2.5 nozzle, plasma gas, 35 slpm (Ar) + 10 slpm (H_2), 600 A, 59 V

flow was found to be generally subsonic (compressible) for the three nozzles when operated at chamber pressures of around or above 50 kPa, as measured by enthalpy probe investigations. However, when the pressure was 27 kPa, the flow condition was supersonic. Emission spectroscopy (absolute intensity) and enthalpy probe techniques exhibited reasonable agreement in the regions of the jet where the local thermodynamic equilibrium (LTE) condition was valid (the core of the jet). Over the entire pressure range of interest (low to high pressure), the Laval nozzles generated plasma jets with extended hot cores compared to a standard cylindrical nozzle. At reduced chamber pressures, e.g., 27 kPa, it was demonstrated that plasma jets issuing from Laval nozzles were not only shock wave free, but they also had higher centerline values of temperature and velocity. These advantages provide for significant improvements to be made to the layer structure and deposition efficiency of spray coatings using dc plasma torches equipped with Laval nozzles.

Acknowledgments

The financial support by the Ministère de lÉducation de la Province du Québec through its FCAR program and Natural Sciences and Engineering Research Council of Canada and by the German Ministry for Education, Science, Research and Technology (BMBF) through its program for scientific and technological cooperation with Canada is gratefully acknowledged. The authors are also grateful to Dr. P. Lanigan for proofreading this article.

References

1. E. Pfender, J.R. Fincke, and R. Spores, Entrainment of Cold Gas into Thermal Plasma Jets, *Plasma Chem. and Plasma Process,* Vol 11, 1991, p 529-543
2. J.R. Fincke, C.H. Chang, W.D. Swank, and D.C. Haggard, Entrainment and Demixing in Subsonic Thermal Plasma Jets: Comparison of Measurements and Predictions, *Int. J. Heat Mass Transfer,* Vol 37, 1994, p 1673-1682
3. R.H. Henne, V. Borck, W. Mayr, K. Landes, and A. Reusch, Influence of Internal Cold Gas Flow and Nozzle Contour on Spray Properties of an Atmospheric Plasma Torch, *Thermal Spray Science & Technology,* C.C. Berndt and S. Sampath, Ed., ASM International, 1995, p 774
4. K. Foelsch, The Analytical Design of an Axially Symmetric Laval Nozzle for a Parallel and Uniform Jet, *J. Aeronaut. Sci.,* March 1949, p 161-168
5. M. Sabsabi, S. Vaquié, D.V. Gravelle, and M.I. Boulos, Emission Spectroscopic Study of a Low Pressure Supersonic Ar-H_2 DC Plasma Jet, *J. Phys. D: Appl. Phys.,* Vol 25, 1992, p 425-429
6. M. Rahmane, G. Soucy, and M.I. Boulos, Analysis of the Enthalpy Probe Techniques for Thermal Plasma Diagnostics, *Rev. Sci. Instrum.,* Vol 66, 1995, p 3424-3431
7. M. Brossa and E. Pfender, Probe Measurements in Thermal Plasma Jets, *Plasma Chem. and Plasma Process.,* Vol 8, 1988, p 75-90
8. W.D. Swank, J.R. Fincke, and D.C. Haggard, Modular Enthalpy Probes and Gas Analyzer for Thermal Plasma Measurements, *Rev. Sci. Instrum.,* Vol 64, 1993, p 56-62
9. J.R. Fincke, S.C. Snyder, and W.D. Swank, Comparison of Enthalpy Probe and Laser Light Scattering Measurements of Thermal Plasma Temperatures and Velocities, *Rev. Sci. Instrum.,* Vol 64, 1993, p 711-724
10. F.P. Incropera and G. Leppert, Investigation of Arc Jet Temperature Measurement Techniques, *ISA Trans.,* Vol 6, 1967, p 35-41
11. W.L.T. Chen, J. Heberlein, and E. Pfender, Diagnostics of a Thermal Plasma Jet by Optical Emission Spectroscopy and Enthalpy Probe Measurements, *Plasma Chem. Plasma Process.,* Vol 14, 1994, p 317-332